ISSN 0027-1349, Moscow University Physics Bulletin, 2018, Vol. 73, No. 1, pp. 89–94. © Allerton Press, Inc., 2018.

CONDENSED MATTER PHYSICS

Exploring the Influence of a Focusing and Gaussian Profile Electron Beam in SEM Imaging through Monte Carlo Simulation[1]

P. Zhang[a, b]

[a] *School of Electronic Information Engineering, Yangtze Normal University, Chongqing, 408003 People's Republic of China*

[b] *School of Pharmacy, Tongji Medical College, Huazhong University of Science and Technology Wuhan, Hubei, 430030 People's Republic of China*

e-mail: zhangp007@foxmail.com

Received July 6, 2017

Abstract—Gaussian profile is conventionally assumed as the probe shape of the incident electron beam in theoretical analysis of dimensional measurements by a scanning electron microscope (SEM). However, it is not suitable for samples with small and tiny structure. In this paper, a model of a focusing electron beam with finite width due to aberration was used in simulating the SEM image of gold particles/balls on a carbon substrate. An effective electron beam shape (EEBS) was displayed and was found that it deviates significantly from the Gaussian profile. The difference between images simulated by Monte Carlo method with ideal electron incident beam, electron beam focusing model and with ideal beam incident then convoluted by Gaussian profile were discussed in detail. Furthermore, the influence of external electric field effect: full extraction and no extraction for imaging were studied.

DOI: 10.3103/S0027134918010174

1. INTRODUCTION

Scanning electron microscopy has been widely used for micrometre and nanometre scale metrology [1]. Electron beam broadening due to aberration is always present, causing a unclear imaging on critical strcutre of samples which seriously influence the dimensional measurement [2]. Effects from this are relatively small with developed aberration corrected SEM set-ups, and might not cause very large errors for large-scale samples. However, they pose a problem with downsizing of semiconductor devices to the nanometre scale. For example, electron beam broadening effects the measurement for trapezoid linewidth singnificantly [3]. Therefore, accurate dimension metrology becomes a very important issue [4].

For this purpose, the method employing Gaussian profile to describe electron beam shape is widely used for theoretical analysis. Specifically, SEM images can initially be simulated with Monte Carlo simulation for an ideal electron beam of vanishing width; further convolution of the simulated image with a Gaussian probe shape has been applied to yield a SEM image for finite probe size in practice [5]. However, this method does not meet the fact. beam effects are due not only to probe size but also to the focusing condition [6–11]. Because of the converging angle of an incident probe, the actual landing probe shape on a sample surface with certain topography varies from place to place. Specimen surface topography thus not only changes the angle of incidence of the primary beam with respect to the local surface normal, but also distorts the 2D distribution at the landing position when it is projected onto a horizontal imaging plane. The shape of this 2D distribution of incident electrons is referred to as the "effective electron beam shape" (EEBS) [6]. Some quantifications of EEBS are as follows. Tanaka et al. [6, 7] have discussed the EEBS for a regular trapezoid line structure with a cone-shaped electron beam focusing model [6] and with a spherical aberration [7]. In our previous paper [3], the EEBS maps for each image pixel of simulated multiple arbitrary shaped Au particles were obtained. It was found that the EEBS is much more accurate than a Gaussian profile to obtain a convoluted image. However, the difference between SEM images with ideal beam incident, ideal beam incident then convoluted by Gaussian shape and that by EEBS is not discussed in detail yet and this is very important for future theoretical analysis.

To this end, a reasonable electron beam focusing model for a Monte Carlo simulation of a SEM image has continuted to be proposed [2, 3]. It exhibits good performance on simulated image contrast in comparison with experiment, and is also easy to implement. On the other hand, recent progress in the Monte Carlo simulation technique has enabled one to model a sample with moderate or even arbitrarily complex sample structure [12–19]. A sophisticated Monte Carlo-based

[1] The article is published in the original.

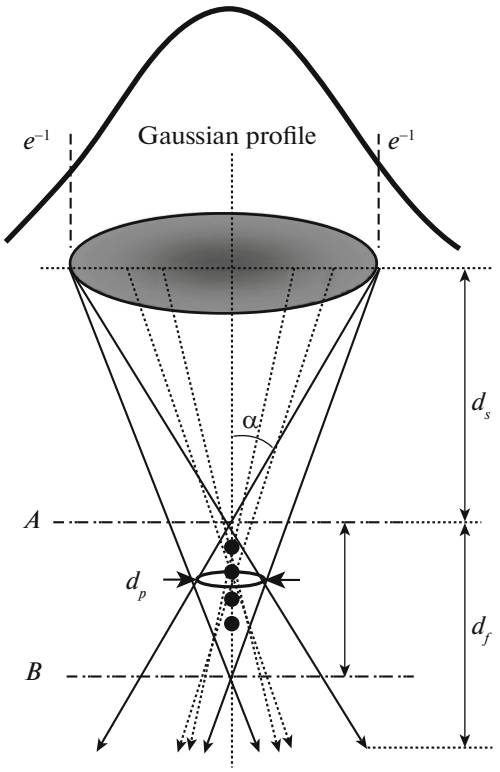

Fig. 1. Schematic diagram of the electron beam configuration in our focusing model. α is the aperture angle, d_f is the distance between the focusing point and the substrate surface, d_s is the distance between the focusing point and a horizontal disc, d_p is the diameter of least confusion disc along the beam axis.

physical model of the interaction of electron beam with the sample, which employs a dielectric functional model for electron inelastic scattering and a Mott cross section for electron elastic scattering, can describe in detail the individual scattering processes of primary electrons in a solid material, and also the cascade production process of secondary electron signals [20]. In this paper, a model of a focusing electron beam with finite width due to aberration was used in simulating the SEM image of gold particles/balls on a carbon substrate. An effective electron beam shape (EEBS) was displayed. The difference between images simulated by Monte Carlo method with ideal electron incident beam, electron beam focusing model and with ideal beam incident then convoluted by Gaussian profile were discussed in detail. Furthermore, the influence of external electric field effect: full extraction and no extraction for imaging were studied.

2. CALCULATION METHOD

2.1. Monte Carlo Model

The movement of electrons in a solid can be described in terms of discrete scattering events. Various Monte Carlo models, depending on the approaches to the treatment of electron elastic scattering and inelastic scattering employed have been proposed. The present study is primarily based on our previous model for the simulation of cascade low energy secondary electrons [20]. The electron elastic scattering is described by Mott's differential cross section [21],

$$\frac{d\sigma_e}{d\Omega} = |f(\theta)|^2 + |g(\theta)|^2 \qquad (1)$$

with the Thomas-Fermi-Dirac atomic potential [22], where the scattering amplitudes $f(\theta)$ and $g(\theta)$ are calculated with a partial wave expansion method.

We adopt a dielectric functional model to treat individual electron inelastic scattering events and the associated secondary electron production. The differential inverse electron inelastic mean free path is given by

$$\frac{d^2\lambda^{-1}}{dqd\omega} = \frac{\hbar}{\pi a_0 E}\,\mathrm{Im}\left\{\frac{-1}{\varepsilon(q,\omega)}\right\}\frac{1}{q}, \qquad (2)$$

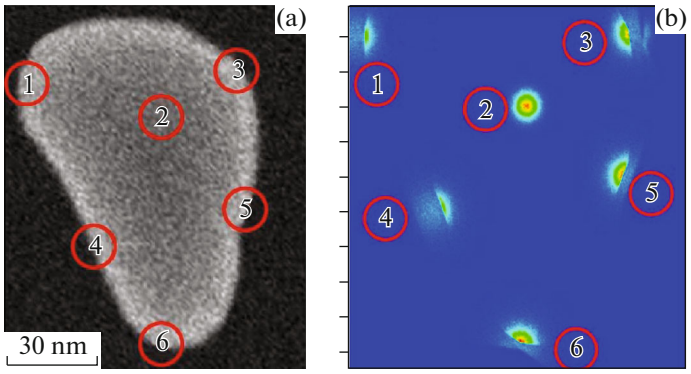

Fig. 2. (a) A simulated SE image of a Au nanoparticle. The primary energy is 1 keV for an electron beam with aperture an angle α of 40 mrad and the focusing position is at substrate; (b) is the 2D electron density distribution, i.e., the EEBS, at the 6 landing positions indicated in (a).

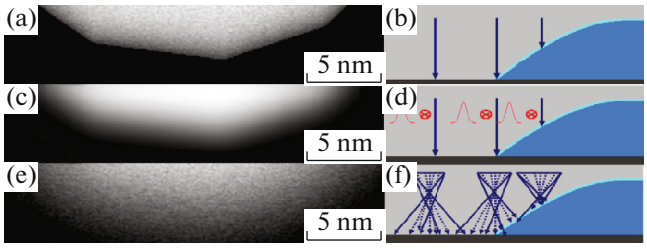

Fig. 3. (a, e) Simulated SE images of an edage of an particles for an ideal primary electron beam of vanishing size and an electron beam focusing model, respectively; (c) the corresponding convoluted images for (a) with a Gaussian profile with FWHM of 5 nm; (b, d, f) the corresponding schematics.

where a_0 is the Bohr radius, $\hbar\omega$ is the energy loss, and $\hbar q$ is the momentum transfer from an electron of kinetic energy E penetrating into a solid of dielectric function $\varepsilon(q,\omega)$. The energy loss function, $\mathrm{Im}\{-1/\varepsilon(q,\omega)\}$, completely determines the electron inelastic scattering channels. It can be obtained by extrapolating the optical energy loss function, $\mathrm{Im}\{-1/\varepsilon(\omega)\}$, into the (q,ω)-plane in a single-pole approximation, as in our previous simulations [20, 23].

However, the single-pole approximation performs poorly in simulations of low energy secondary electrons for free electron-like materials. Therefore, in this work we employ the full Penn algorithm [24] to calculate the energy loss function with the Lindhard dielectric function $\varepsilon_L(q,\omega,\omega_p)$,

$$\mathrm{Im}\left\{\frac{-1}{\varepsilon(q,\omega)}\right\} = \int_0^\infty d\omega_p g(\omega_p)\,\mathrm{Im}\left\{\frac{-1}{\varepsilon_L(q,\omega;\omega_p)}\right\}, \quad (3)$$

where the expansion coefficient $g(\omega)$ is related to the optical energy loss function by $g(\omega) = (2/\pi\omega)\,\mathrm{Im}\{-1/\varepsilon(\omega)\}$. The expansion basis, i.e., the Lindhard energy loss function $\mathrm{Im}\{-1/\varepsilon_L(q,\omega)\}$, is made up two parts corresponding single electron excitation and plasmon excitation:

$$\mathrm{Im}\{-1/\varepsilon_L(q,\omega)\} = \mathrm{Im}\{-1/\varepsilon(q,\omega)\}_e + \mathrm{Im}\{-1/\varepsilon(q,\omega)\}_{pl}. \quad (4)$$

Each excitation in the equation above can be analytically evaluated [25], and a database of optical constants [26] was used in the calculation.

2.2. Electron Beam Model

The electron probe shape and the beam focusing is model as schematically shown in Fig. 1, where α is the aperture angle. The focusing position is specified by the distance, d_f, measured from the substrate surface; it is defined such that $d_f < 0$ corresponding to underfocus, and $d_f > 0$ corresponding to over-focus. The focusing point is broadened into a disk of least confusion along the beam axis, which specifies the electron beam size due to the aberrations of the objective lens. The diameter of this disk is the electron probe diameter, d_p whose value varies with α and beam energy; we use the d_p-value and the α-value for analysis according to the functional relationship shown in Fig. 2.14 of [27].

For model the beam focusing effect we first must determine the incident direction of an electron trajectory within a primary beam. In our simulation all of the primary electron trajectories start from a horizontal plane which is separated from the focusing point by the distance d_s (Fig. 1). The position of these electrons is distributed in a two-dimensional (2D) Gaussian profile; the diameter of the horizontal disc of the electron beam is $d_s \tan\alpha$, where the electron density drops to $1/e$ of the profile maximum. The incident electron rays are determined by the following method: firstly, the upper and lower limits, for the ray crossover,

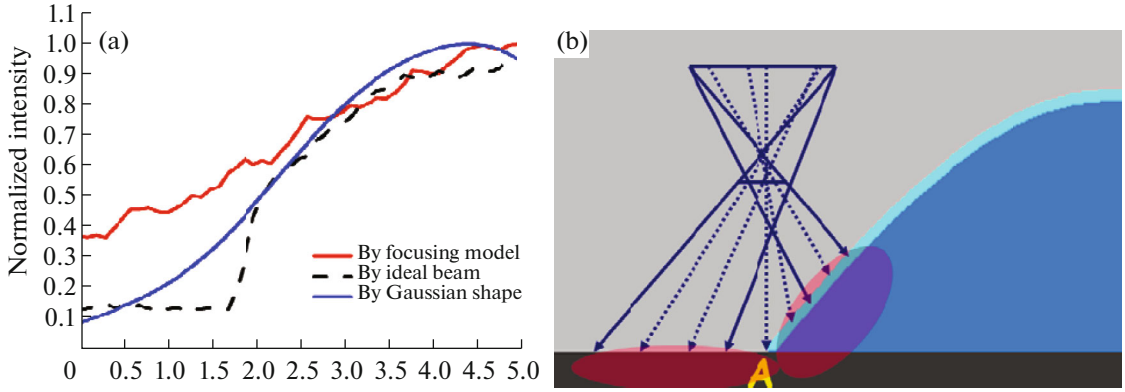

Fig. 4. (a) A comparison on the line profiles, the vertical lines crossing the centre of horizontal axis, extracted from Figs. 3a, 3c, 3e. The intensity values have been normalized; (b) a schematic of using an electron beam focusing model.

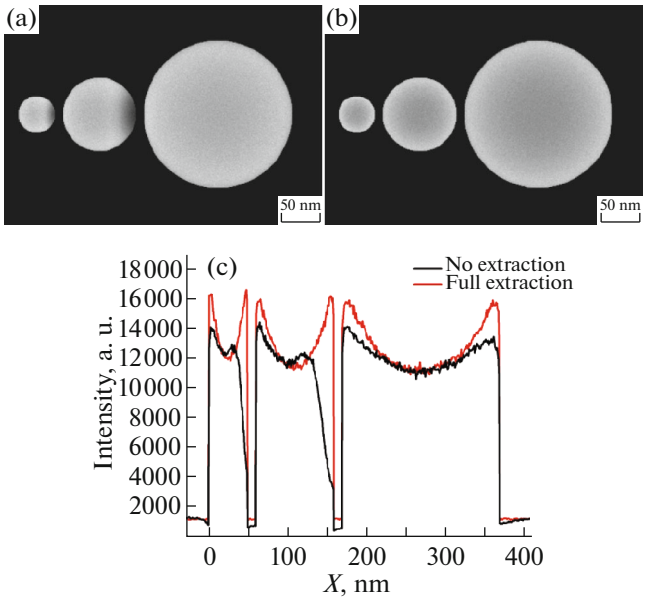

Fig. 5. Two detection modes: no extraction mode and full extraction of Au particles SE images. The samples are ideal spherical shape. The primary electron energy is 1 keV. (a) No extraction, (b) full extraction, (c) a comparison on the line profiles, the horizontal lines crossing the centre of vertical axis, extracted from (a, b).

A and B are determined according to the geometric relationship between d_p and d_s, where d_s represents the working distance (this is several millimeters in most scanning electron microscopes, such as the Hitachi S-4800 field emission SEM and the Hitachi S-3400N-II SEM, and is taken to be 5 mm here). Next the position of an electron incident ray on the beam axis and at the focusing point is randomly and uniformly selected in the range of values between A and B. Finally, the ray is formed by connecting the two positions on the horizontal plane and at the focusing point (Fig. 1). In this model, the correlation between the coordinates of the two points in the upper disc and on the beam axis is negligible if d_s is large. The resultant beam profile has been demonstrated to be reasonable for under-focusing, focusing, and over-focusing cases [2].

3. RESULTS AND DISCUSSION

3.1. EEBS on Au/C System

Because EEBS cannot be experimentally measured, in order to display the EEBS clearly, an arbitrarily-shaped gold particle island on a carbon substrate were constructed using finite element mesh model [5]. This sample structure was then employed in a Monte Carlo simulation, which employed a space subdivision for trajectory tracing acceleration in order to improve the computational efficiency for this finite element meshed sample structure [5]. Figure 2b displays the 2D density distribution of primary electrons landing at the sample surface and projected onto the substrate plane, i.e., the EEBS studied here, at 6 locations as indicated in Fig. 2a. The primary energy is 1 keV for an electron beam with aperture an angle α of 40 mrad and focusing position is at substrate. It is very clear that the EEBS shapes are quite different. They

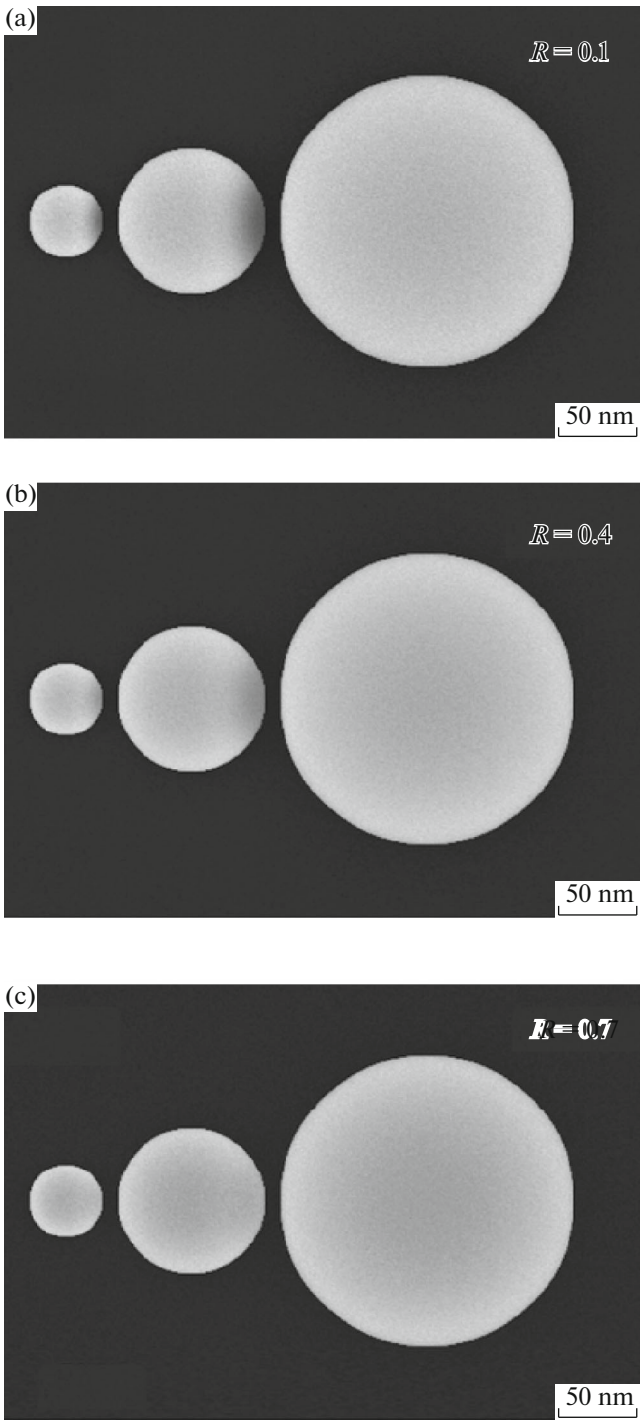

Fig. 6. The effect of the different extraction parameter values in simulations. R = (a) 0.1, (b) 0.4,(c) 0.7.

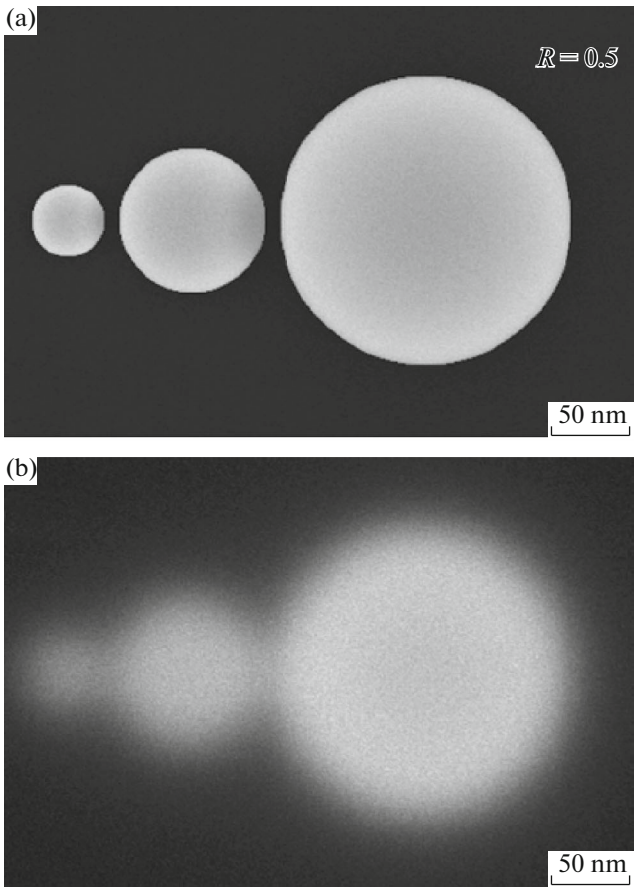

Fig. 7. (a) A simulated result of deal spherical shaped Au particles SE images when R value is 0.5; (b) a simulated result with the condition for $d_f = 0.11$ μm, $\alpha = 30$ mrad.

strongly depend on the spot size and the local topography. Therefore, the EEBS can be totally different from the constant Gaussian shape that is usually assumed over the scanning area. Only in the case of a location is at the flat area (the position maked "2" in Fig. 2a) can the distortion of the EEBS from a Gaussian profile be neglected. In [3], the quantitative difference between EEBS and Gaussian shape was discussed.

We further studied the difference between SEM images for an ideal primary electron beam of vanishing size and an electron beam focusing model as well as ideal beam incident then convoluted by Gaussian shape (FWHM of 5 nm). As shown in Figs. 3a, 3c, 3e, the image with the ideal beam is very distinct and sharp and that with convoluted by Gaussian shape becomes smooth and indistinct. However, image with an electron beam focusing model presents a big difference from them. The edge displays a uniform transition which will cause a blurry judgement for the dimension measurement. Therefore, large different critical measurement results will be obtian if adopting Gaussian shape to describe elelctron beam.

Figure 4a displays the quantitative comparison on the vertical line crossing the centre of horizontal axis from the Figs. 3a, 3c, 3e at the same position. The intensity values have been normalized. The figure confirms the above qualitative conclusion by comparing image contrast. Figure 4b is a schematic to show the reason why if using an electron beam focusing model cannot present a distinct and sharp and much more blurry than using Gaussian shape. Because as shown in Fig. 4b, with the aperture and focusing effect, the landing spot at A point, is expanded, just liking a light beam lighting up the slit.

3.2. External Electric Field Effect

Figures 5a, 5b respectively shows the two detection modes: no extraction mode and full extraction of Au particles SE images. The samples are ideal spherical shape. In the no extraction, the left and middle balls present the shading effect, i.e., the darker brightness at the edge facing the gap. This is because that SEs which emerge from one sample are assumed to travel in straight lines and may reenter the neighboring samples along their paths. It could make the low energy SE signal loss. However, modern SEM equipments employ the strong external electron fields to extract more SEs to the detector. To emulate this, in the full extraction, we count the SEs as soon as they emerge the sample or the substrate, no longer reenter another structures. As Fig. 5b shown, at the same positions where have shading effect in Fig. 5a present symmetrical brightness at the edge. Figure 5c shows the comparison on the line profiles, the horizontal lines crossing the centre of vertical axis, extracted from Figs. 5a, 5b. It can be seen that both in the shading/non-shading edges, the profile intensity in the full extraction mode are higher than no extraction. In additional, the intensity of the biggest Au ball's right edge is also higher in full extraction than no extraction. That is because the emerged SEs travel into substrate than exict a lower SE yield in no extraction rather than shading effect. An extraction parameter can thus be applied to tune the contrast between that without extraction and that with full extraction [28]. In here, R is the extraction parameter (between 0 for no extraction and 1 for full extraction). Figures 6a–6c shows the effect of the different extraction parameter values in simulations. As the R value increases, the shading effect becomes disappearing. These can be approximately reflected the effect of different external electric filed values. Figure 7a shows a simulated result when R value is 0.5. However, focusing primary electron beam with finite width due to aberration may be like a light to shine the darkness of shading region. It may be present the same result with or without external electric field. Figure 7b demonstrates this assumption. This figure shows a simulated result with the condition ($d_f = 0.11$ μm, $\alpha = 30$ mrad). The results are almost the same. There is no shading effect.

CONCLUSIONS

Based on a sophisticated Monte Carlo physical model and electron probe model, a focusing electron beam with finite width due to aberration was used to simulate the SEM image for a gold particle/balls on a carbon substrate. The simulation allowed us to obtain the EEBS maps for each image pixel, by counting the number of electrons landing on the structure at nearby pixels. The maps are shown to be strongly dependent on the local topography of the sample, and are therefore very different from the Gaussian probe which is assumed to be invariant with position. The difference between images simulated by Monte Carlo method with ideal electron incident beam, electron beam focusing model and with ideal beam incident then convoluted by Gaussian profile were discussed in detail. If using an electron beam focusing model, with the aperture and focusing effect, the landing spot at a point, is expanded, just liking a light beam lighting up the slit. The effect of different external electric filed conditions can be approximately reflected by a extraction parameter.

ACKNOWLEDGMENTS

We thank the support from 2016 Wuhan government doctoral funding program and the start-up research funding of Yangtze Normal University (no. 2017KYQD113).

REFERENCES

1. Z. Wang, K. K. Seet, R. Fukaya, Y. Kadowaki, N. Arai, M. Ezumi, and H. Satoh, Proc. SPIE **6730**, 67304T (2007).
2. P. Zhang, S. F. Mao, Z. M. Zhang, and Z. J. Ding, Proc. SPIE **8729**, 87290K (2013).
3. P. Zhang, S. F. Mao, and Z. J. Ding, Eur. Phys. J. Appl. Phys. **69**, 30703 (2015).
4. https://www.semiconductors.org/clientuploads/Research_Technology/ITRS/2007/ERM.pdf
5. P. Zhang, H. Y. Wang, Y. G. Li, S. F. Mao, and Z. J. Ding, Scanning **34**, 145 (2012).
6. M. Tanaka, J. S. Villarrubia, and A. E. Vladar, Proc. SPIE **5752**, 144 (2005).
7. M. Tanaka, C. Shishido, and H. Kawada, Proc. SPIE **6152**, 61523Z (2006).
8. C. Shishido, R. Nakagaki, M. Tanaka, Y. Takagi, H. Morokuma, O. Komuro, and H. Mori, Proc. SPIE **5038**, 1071 (2003).
9. R. Attota, R. Silver, and R. Dixson, Appl. Opt. **47**, 495 (2008).
10. C. Wang, J. Meinhardt, and P. Loebmann, J. Sol-Gel Sci. Technol. **53**, 148 (2010).
11. M. Daneshpanah, G. Abramovich, K. Harding, and A. Vemury, Proc. SPIE **8043**, 80430G (2011).
12. T. Prill and K. Schladita, Scanning **35**, 189 (2013).
13. Z. Ruan, S. F. Mao, P. Zhang, H. M. Li, and Z. J. Ding, Proc. SPIE **8729**, 87290J (2013).
14. C. G. Frase, D. Gnieser, and H. Bosse, J. Phys. D: Appl. Phys. **42**, 183001 (2009).
15. N. W. M. Ritchie, Surf. Interface Anal. **37**, 1006 (2005).
16. A. Seeger, C. Fretzagias, and R. Taylor, Scanning **25**, 264 (2003).
17. H. Yan, M. M. El Gomati, et al., Scanning **20**, 465 (1998).
18. J. R. Lowney, Scanning **17**, 301 (1996).
19. J. R. Lowney, Scanning **17**, 281 (1995).
20. Z. J. Ding and R. Shimizu, Scanning **18**, 92 (1996).
21. N. F. Mott, Proc. R. Soc. London A **124**, 425 (1929).
22. R. A. Bonham and T. G. Strand, J. Chem. Phys. **39**, 2200 (1963).
23. Z. J. Ding, X. D. Tang, and R. Shimizu, J. Appl. Phys. **89**, 718 (2001).
24. D. R. Penn, Phys. Rev. B **35**, 482 (1987).
25. K. O. Jensen and A. B. Walker, Surf. Sci. **292**, 83 (1993).
26. *Handbook of Optical Constants of Solids*, Ed. by E. D. Palik (Academic, New York, 1997), Vol. 2.
27. L. Reimer, *Scanning Electron Microscopy*, 2nd ed. (Springer, New York, 1998), p. 32.
28. A. Seeger, C. Fretzagias, and R. Taylor, Scanning **25**, 264 (2003).